JOURNAL OF MATERIALS SCIENCE 25 (1990) 223–232

Iron species in fusion-cast, glassy-phase-containing corundum materials; EPR and susceptibility analyses

REINHARD STÖSSER
Department of Chemistry, University of Humboldt, Bunsenstr 1, Berlin 1080, GDR
RUDOF BRENNEIS
Central Institute of Inorganic Chemistry of the Academy of Sciences of the GDR
INES EBERT
Central Institute of Physical Chemistry of the Academy of Sciences of the GDR

By means of EPR, susceptibility, EMP, light-microscopic, thermal and chemical methods the influence of production conditions and subsequent treatments on glassy-phase-containing corundum materials were studied. Melting of the system (Al_2O_3, SiO_2, Na_2O, Fe_3O_4) under reductive conditions leads to a reduction of Fe^{3+} species contained to Fe^{2+} and even to Fe^0 clusters with ferromagnetic behaviour. Both species markedly influence the mechanical properties of the material by increase of their volumes in consequence of oxidation in subsequent thermal processes. The following model with regard to the localization of the iron species in the system ensues: Fe(III) in corundum, Fe_2O_3, Fe_3O_4 and (scarcely) in the glassy phase; Fe(II) in the glassy phase, $FeAl_2O_4$ (hercynite) as a solid solution in corundum, and Fe_3O_4; (Fe^0) clusters in corundum. It is therefore not surprising that grinding of the compact material considerably alters the magnetic properties of the samples.

1. Introduction

Fusion-cast, glassy-phase-containing corundum blocks are used in the glass industry for the palisades of glass tank furnaces. The thermal and mechanical properties of these refractories are markedly influenced by comparatively low iron impurities when reductive conditions prevail during fusion in the electric-arc furnace. Thus the quality of the blocks may be considerably decreased. In contrast to corundum containing different dopants [1–5], no spectroscopic and magnetic tests concerning glassy-phase-containing materials have been undertaken so far.

The systems analysed in this paper are of the composition indicated by I_x in Fig. 1. Taking into account the iron impurity component one may expect that the fusion and cooling conditions (see Fig. 2) strongly influence the properties of the castings. An analysis of the standard heats of formation of the system components and the impurities included reveals (Fig. 3) that the iron oxides should be of the lowest thermodynamic stability towards reduction through the carbon of the electrodes used. Consequently it must be expected that iron in a different state of oxidation and coordination is incorporated in the corundum and the glassy phase or that it constitutes independent Fe–O phases*. Only little is known about the influence of the approximately 10% of the comparably low-melting glassy phase ($T_g \approx 750°C$) on these phenomena. Since the overall iron concentraion (see Table I) does not exceed the range of 0.7 wt % FeO_3, even if iron compounds are added to the melt, diffraction and phase-analytical methods are not suited for a solution of the problems mentioned. The aim of the present paper was to arrive at statements concerning the oxidation state of the iron, its localization and function, by means of magnetic methods electron paramagnetic resonance (EPR) and susceptibility) in combination with chemical, EMP and light-microscopic methods. Moreover, it was intended to draw conclusions on the formation of individual phases during the cooling down of the melt or during subsequent loads. It is particularly from the latter that indications of the involvement of iron species in the initiation and the course of crack formation of the castings were expected.

2. Experimental procedure

The blocks were fused from a starting mixture of Al_2O_3, SiO_2 and Na_2O in a open electric arc furnace with graphite electrodes. To intensify the effect of iron impurities, Fe_3O_4 or Fe_2O_3 was added to the mixtures II to IV (Table I). The conditions for melting and cooling down the charges are summarized in Fig. 2†.

*According to the FeO_x–Al_2O_3 phase diagram (Fig. 1) a spinel phase (hercynite) is possible too.
†The term "residence time" means here the time from casting the melt into casting box till the moment of setting the block into an isolation powder.

0022–2461/90 $03.00 + .12

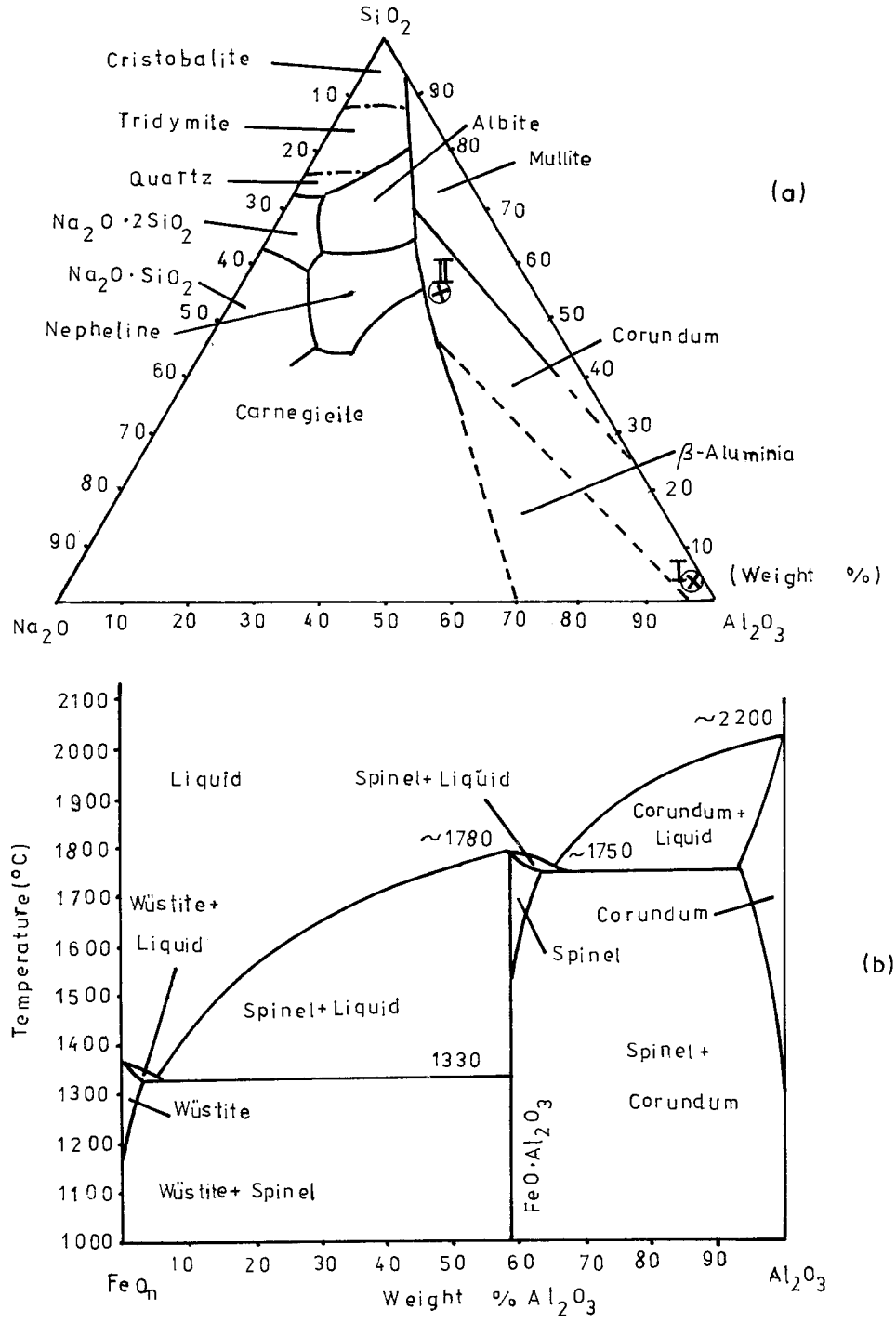

Figure 1 Phase diagrams: (a) Na_2O–Al_2O_3–SiO_2 (Osborn and Muan [6]); (b) FeO_n–Al_2O_3 [7].

Sample V was fused in a closed electric arc furnace. The iron content of the samples was estimated by chemical analysis with respect to the Fe(II), Fe(III) and overall iron contents (Table I). As preliminary investigations [9] show, grinding of the samples leads to significant alterations and destruction of structure of components other than α-Al_2O_3 and to drastic changes of the magnetic properties of the resulting powders (see Fig. 10 (below)). In particular, the glassy phase and various independent FeO_x phases (Section 3) are affected by the grinding process. To overcome these difficulties, from the central part of the blocks rod-like samples (3 × 3 × 50 mm) were sawn out. From the same part of the blocks samples were taken for the microscopic and EMP investigations. Despite the grinding effects, thermal, mechanical and chemical (HCl 37%, HF 40%) treatments were carried out on powders (grain size $< 60\,\mu$m). The annealing time was on the average 15 to 2 h. Sample I was used as a standard for comparison and compensation in the electron spin resonance (ESR) and magnetic measurements. Sample I represents a material of good quality (0.06 wt % Fe_2O_3) which is produced from a starting material containing only few impurities. Under the production conditions summarized in Fig. 2, Sample I is produced with the expected thermal and mechanic properties. The ESR measurements were carried out in the temperature range 77 to 300 k at different microwave powers ($10^{-5} < P_{MW} < 2 \times 10^{-1}$ mW) on two instruments: type E_4 (Varian, USA) and ERS 230 (ZWG of the Academy of Sciences of the GDR). Measurements of the static magnetic susceptibility of

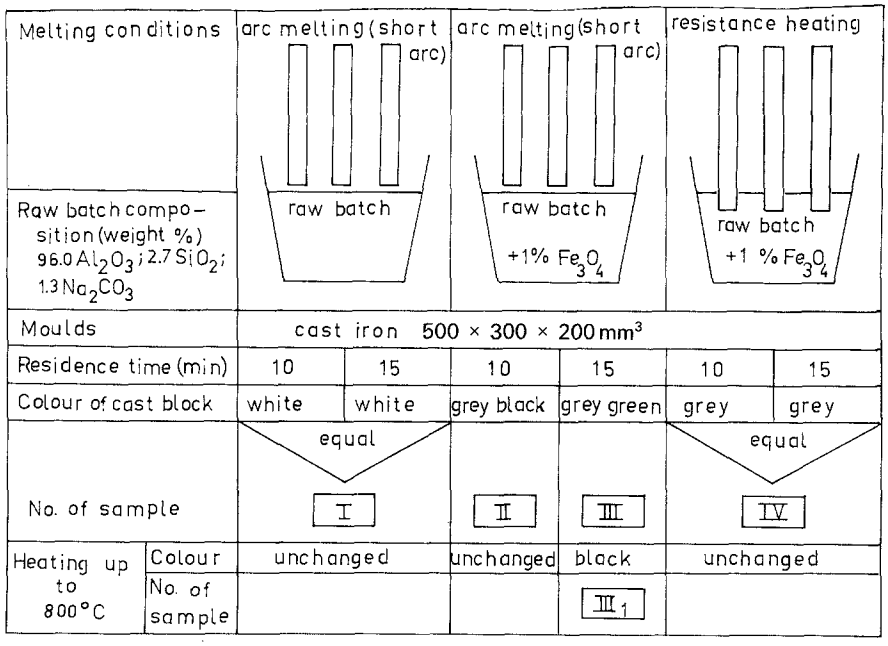

Figure 2 Manufacturing conditions for glassy-phase-containing corundum blocks.

the rod-like samples were performed by the help of a modified Gouy balance [10] equipped with a horizontal balance system. For the compensation of the diamagnetic part of the samples (α-Al_2O_3 and glassy phase) and of small concentrations of included paramagnetic impurities an arrangement as illustrated in Fig. 4b with sample I as compensation was used. Samples with well-known susceptibilities were selected to calibrate the pendulum weighting [10], yielding the difference susceptibility $\Delta\chi_g = \chi_g(X) - \chi_g(\mathrm{I})$ (Fig. 4a).

3. Results and discussion

3.1. Susceptibility measurements

The $\Delta\chi_g$ values of the bars from samples I to V are plotted against the magnetic induction $\boldsymbol{B}_0$ in Fig. 4. Curve I relates to the uncompensated sample I and directly furnishes $\chi_g = f(\boldsymbol{B}_0)$ ($\chi_g = -0.22 \times 10^{-6}$). The expected quadratic dependence of $\boldsymbol{B}_0$ is approximately fulfilled; I is diamagnetic as a whole. For II and the standard sample V fused in the closed furnace (Table I) there is–due to the higher iron concentration–paramagnetic behaviour superimposed on minor contributions of collective magnetic effects. Sample III, however, shows a higher proportion of paramagnetism and an increase of the constituents with magnetic order. There are much larger deviations from the purely paramagnetic behaviour. As may already be expected due to the dark appearance of III_1, the existence of magnetically ordered regions is clearly substantiated by curve III_1 as well as the respective EPR spectra. Taking into consideration other results (e.g. the Fe(II)/Fe(III) relationship, see Table I) it is possible to class them with a magnetic-

TABLE I Content of iron by chemical analysis (wt %)

Sample	Fe(II)	Fe(III)	Σ Fe_2O_3
Compact materials			
I	0.03	0.03	0.06
II	0.42	0.1	0.55
III	0.56	0.03	0.65
III_1	0.35	0.26	0.65
IV			0.19
V	0.47	0.08	0.6
Powders, only heat-treated			
III (500° C)	0.55	0.06	0.68
III (600° C)	0.45	0.18	0.68
III (700° C)	0.22	0.45	0.69
III (800° C)	0.22	0.44	0.68
III (1000° C)	0.07	0.57	0.65
III (1200° C)	0.02	0.63	0.65
III (1400° C)	0.27	0.38	0.65
Glassy phase*			
(a)	0.3	0.22	0.56
(b)	0.38	0.15	0.58

*(a) Separately fused glassy phase oxidizing conditions with molar ratio of Al_2O_3: Na_2O = 1.45;
(b) as (a) with reductive conditions and a ratio of 1.66.

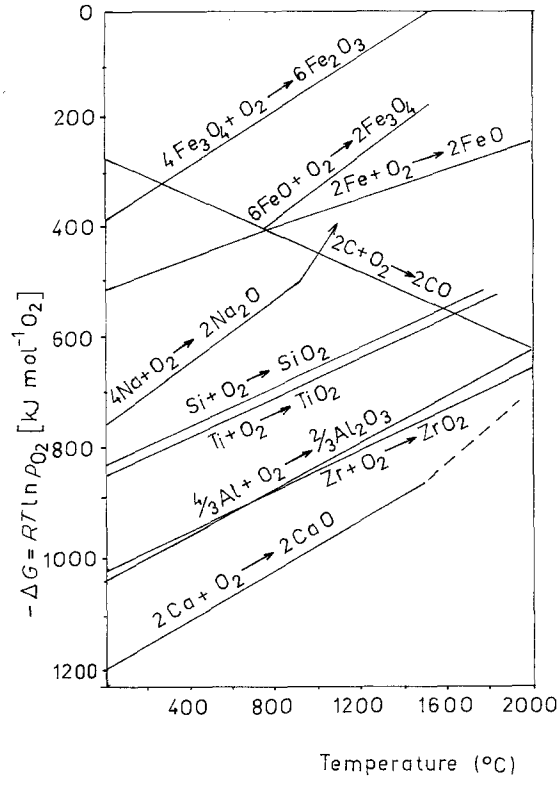

Figure 3 Richardson–Jeffes diagram for some oxides [8].

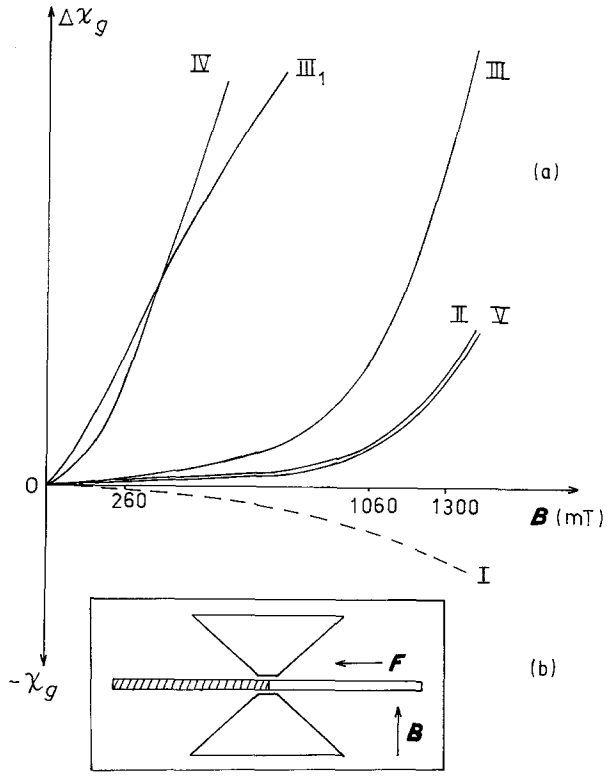

Figure 4 (a) Difference susceptibility $\Delta\chi_g$ of rod-like samples as a function of the static magnetic induction B_0 at 300 k; (b) scheme of experimental arrangement for the $\Delta\chi_g$ measurement F = force on the balance system; hatched part = sample I.

like phase (see also Figs 5 and 6). Sample IV (Fig. 7) shows an even stronger trend towards magnetic order and–together with the EPR results and the ESMA plot–it allows one to deduct magnetic regions constituted by an $(Fe^0)_n$ phase. Here there is no direct indication of a magnetic-like Fe–O phase (see also the grey colour of the sample.

3.2. EPR on rod-shaped samples of the compact material

One may expect EPR signals (X-band) in the range of 0.05 to 0.6 T if Fe^{3+} ions are inserted into the host lattice of polycrystalline samples of α-Al_2O_3 whereby the regions of transition show signal intensities with effective g factors such as $g' = g_{eff} \approx 13$; ≈ 6; ≈ 5.1; ≈ 2.4; and ≈ 2 which are usually easy to evaluate (see also [9]). Other transitions of low intensity can be determined at high field [1, 2, 9, 11]. The latter are of secondary importance for the discussion in this paper.

In the case of low Fe^{3+} concentrations there is the largest intensity in the ESR spectrum of the transition, namely $g \approx 13$. It is an allowed transition between a pair of Kramers doublets [11, 12]. From analyses of monocrystals, the splitting of the Kramers doublets of Fe^{3+} in α-Al_2O_3 is given by Δ_1 (T = 290 K) = 11.768, and Δ_2 = 18.873 GHz [11, 12] whereby Δ_1, for example, increases with the temperature. Thus causes a shift of the transition to higher field (or lower g') in

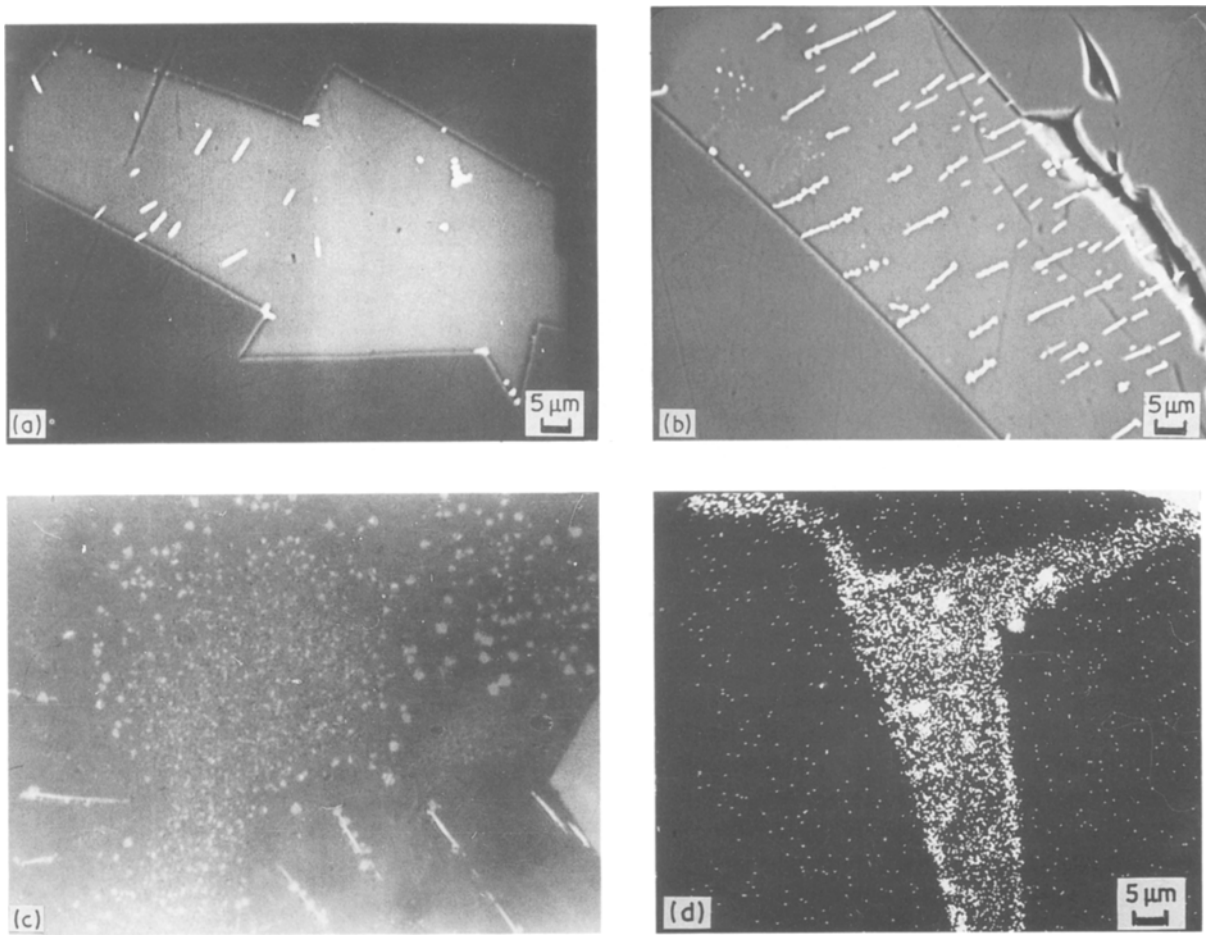

Figure 5 Separations of secondary corundum and magnetite in the glassy phase. (a) For purpose of comparison, the glassy phase of III with only few crystals of secondary corundum (backscattered electron photograph). (b) III: backscattered electrons photograph (c) III: photomicrograph, × 1136. (d) III_1: electron microprobe result (iron scan) on corundum (left, right) and, glassy phase (middle).

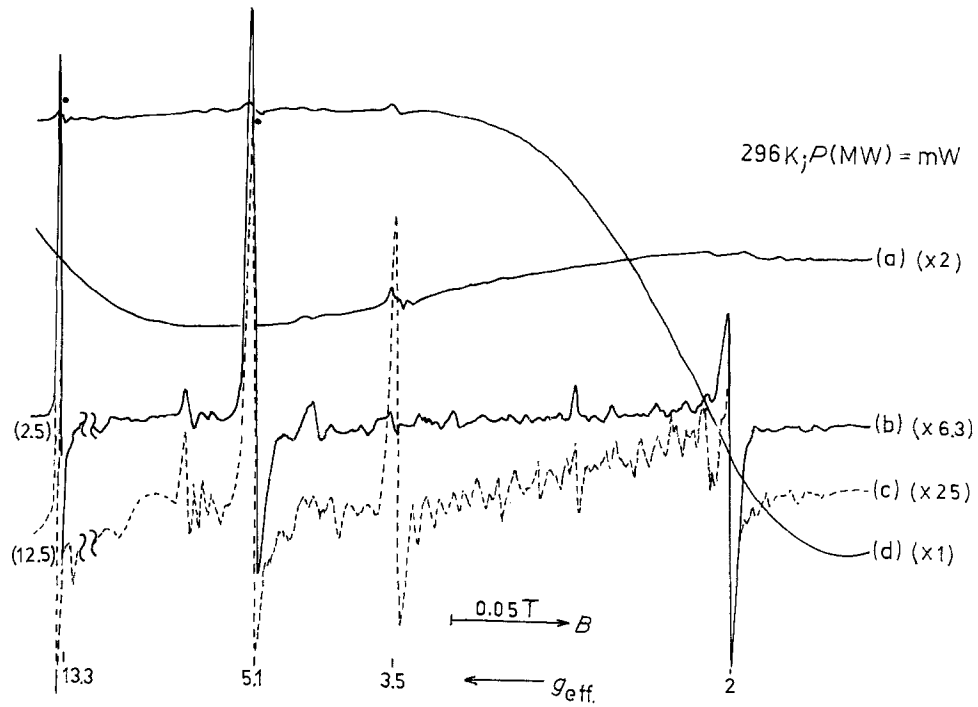

Figure 6 ESR spectra of rod-like samples of (a) IV, (b) I (c) III, (d) III_1.

the X-band. This occurs in all samples analysed; e.g. for sample III $g' = 13.59$ (300 K) and $g' = 12.25$ (77 K). An analysis of the transitions in polycrystalline α-Al_2O_3 samples (e.g. bars or powder) 13–15 results in an image of medium axial distortion of the Fe^{3+} environment in all samples (two non-equivalent Fe^{3+} ions [11]), i.e. $D \approx 0.2\,cm^{-1}$ and $E \approx 0$.

De Biasi and Rodrignes [4, 5] find $g' \approx 5.1$ for the transition which is of the largest integral intensity in the case of Fe^{3+} concentrations > 0.16 wt % in α-Al_2O_3. According to Dowsing and Hasa [13, 14] the following transitions $(5/2)(1/2)(3/2) \rightarrow 5/2(1/2)(3/2)$; $-1/2 \rightarrow 3/2$ contribute to the absorption in the region of $g \approx 5.1$. Hence it follows that the transitions at $g' \approx 13$ and 5.1 do not necessarily respond in the same way to structural changes of the corundum host lattice including different Fe^{3+} concentrations, due to their different physical nature. Obviously the transition at $g' \approx 13$ in the case of Fe^{3+} concentrations of < 0.05 wt % has the smallest line-width in the spectrum and – taking into account the transition probability – the largest intensity. Worth mentioning is the fact that the intensity at $g' \approx 13$ is clearly abve that at 5.1 (see Figs 6 and 8 in all samples analysed, which is in contrast to more concentrated samples [3–5] or to those annealed at 1350° C with the addition of Fe_2O_3 in the frame-work of this study. All samples

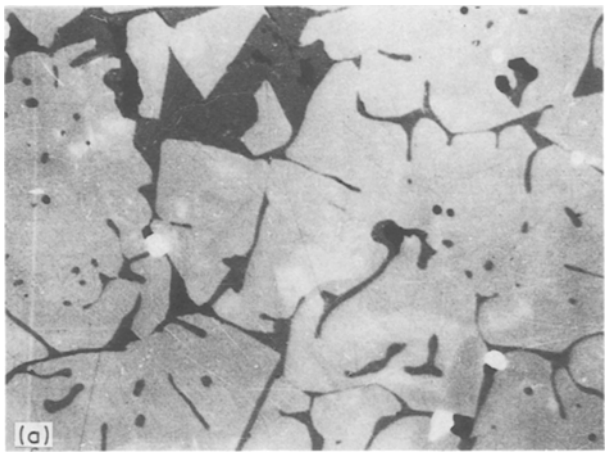

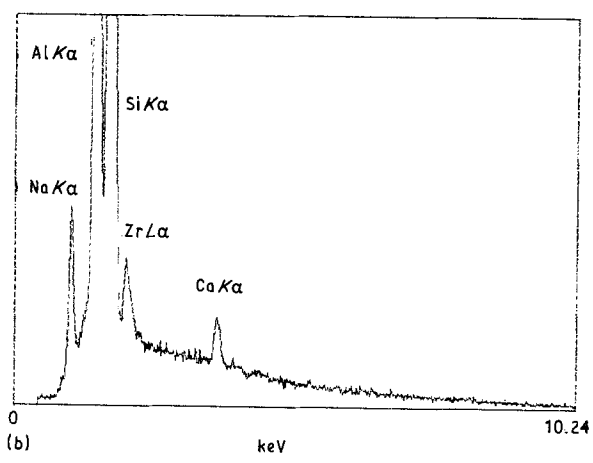

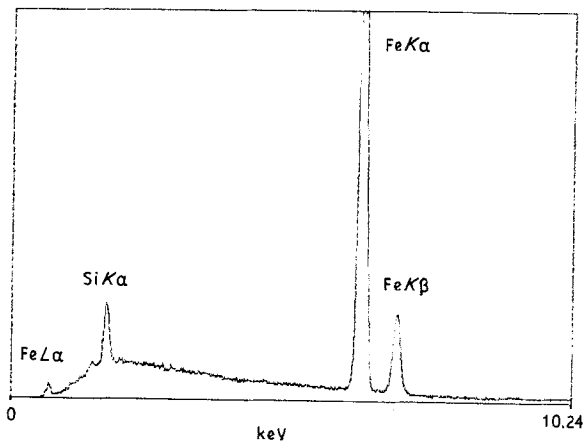

Figure 7 Sample IV. (a) Photomicrograph, magnification × 112 (light grey: corundum, dark grey: glassy phase, black: pores, white: metallic phase. (b) EDS: X-ray peaks of the glassy phase. (c) EDS: X-ray peaks of the metallic phase.

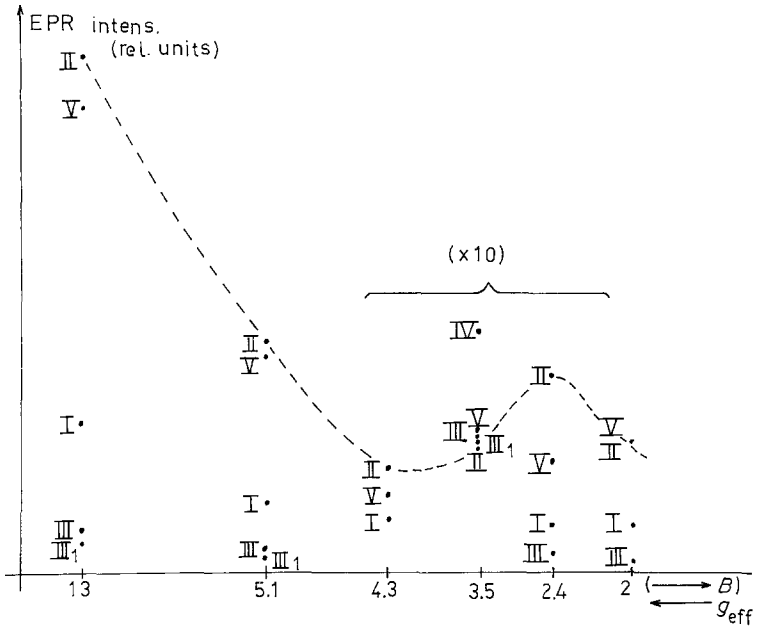

Figure 8 ESR intensities of rod-like samples I to V at 296 k.

with the exception of IV (see below) show comparable relations between the intensities too (see Figs 6, 8, 9 and 10).

Confining the discussion first to the transition at $g' \approx 5.1$, one can qualitatively state a direct proportionality between the EPR intensities and the Fe^{3+} concentrations in the α-Al_2O_3 lattice, whereby minor variations in the line-width are neglected. In this, the following graduation ensues:

$$II \approx V > I > (III \approx III_1) \ldots IV \qquad (1)$$

There have not been detected any Fe^{3+}-signals for Fe^{3+} in the α-Al_2O_3 of sample IV fused under very reduced conditions, although Fe_3O_4 had been added (Table 1 and Fig. 7). However, the relatively high intensity of the transition at $g \approx 3.5$ (see Figs 6 and 8 is remarkable.

From Figs 6, 8 and 9 it may be deduced that a medium Fe^{3+} concentration is present in the corundum in spite of the very low overall concentration of iron in sample I. In the case of an increased supply of iron (e.g. II) the proportion of incorporated iron will grow. This trend has also been confirmed by sample V.

Samples cooled down faster (see Fig. 2) (e.g. III) contain lower Fe^{3+} concentrations in the α-Al_2O_3 that can be spectroscopically observed by EPR. Obviously the incorporation was limited as to time, and the possibility of the oxidation of Fe^{2+} in the melt during the cooling-down period was additionally limited. The chemically ascertained overall concentration of Fe^{3+} in III (see Table I) in comparison with other samples is considerably lower. Annealing the compact material at 800° C (see also Fig. 11) results in III_1 with magnetic properties largely differing from III (see Table I) and Figs 4 and 6. However, there is little change of the Fe^{3+}

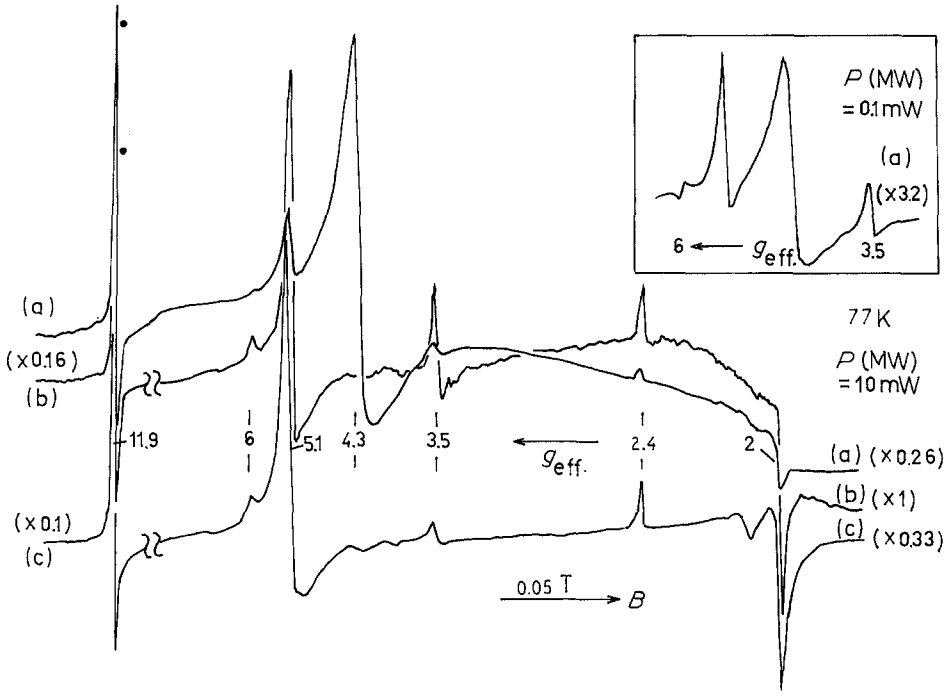

Figure 9 ESR spectra of powders (ground in a W_2C beaker): (a) III after a treatment with HCl; (b) III A_5; (c) III C_2 (see Fig. 11). Inset: microwave power dependence in the region $g > g' > 3.5$

concentration in the α-Al_2O_3. Fig. 5 and the magnetic measurements as well as the chemical analyses (Table I) show that the heat treatment (800° C) causes the separation of secondary corundum and magnetite in the glassy phase. ESR signals were observed in addition to the α-Al_2O_3/Fe^{3+} signals. Those at $g' \approx 4.2$ can be classified as Fe^{3+} ions in the glassy phase or – to a secondary degree–with Fe^{3+} at rhombic-distorted lattice points (e.g. at the corundum surface and the like).

The relative signal intensity at $g' \approx 4.2$ is low in the rods and graduates like that of the Fe^{3+} in the Al_2O_3. Grinding increases the intensity at $g' \approx 4.2$ markedly, which above all can be explained by an oxidation of the Fe^{2+} in the glass. The glassy phase is most strongly strained after the grinding.

The transition at $g' \approx 3.5$ with the comparatively small line-width (ΔB_{pp} = 2 to 5 mT) obviously represents another species inserted into α-Al_2O_3 or an dependent Fe–O_x phase or Fe^{2+} see for example [12, 16] (narrow ESR lines are also possibly caused by small ferromagnetic particles of a diameter $d < 10$ pm) [15]. This signal increasingly occurs with reductively fused samples, i.e. with IV, to a smaller degree with II, V, III and III_1, and at very low intensity with I.

3.3. EPR of selected powders within the range 0 to 0.33 T

The largest intensity of the EPR signals of α-Al_2O_3/Fe^{3+} for sample II is observed with a scarcely changed spectral habit (see Figs. 9 and 10). What can additionally be identified in the glass is the signal of a further impurity (e.g. with $g' = 3.5$), but hardly of Fe^{3+}. After removal of the glassy phase with HF and annealing the sample at 1200° C a considerable increase in the intensity of the α-Al_2O_3/Fe^{3+} signals can be observed. One explanation of this increase is the growth of the Al_2O_3 relative fraction after the extraction. Fig. 10 shows a selection of samples for the purpose of illustrating further intensity effects of the EPR powder spectra.

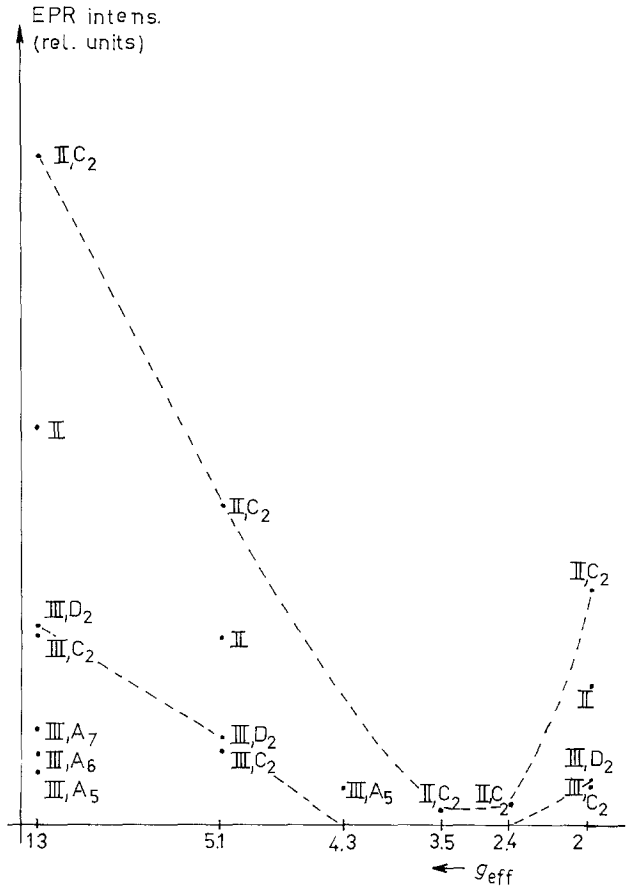

Figure 10 ESR intensities of powders for the treatments shown in Fig. 11 lines (– – –) indicates the relationship of signals from one sample.

3.4. Iron species in the glassy phase

The concentration of Fe^{3+} ions in the glassy phase which is separated as a matrix during the cooling down of the melt is relatively low in all samples. Distinct absorptions at $g' \approx 4.3$ can only be observed in sample A_3 (Fig. 11). In principle, the glassy phase is a reservoir for the deposition of corundum in the systems analysed, due to its saturation with Al_2O_3. As Fig. 5a shows, the glassy phases of III and III_1 contain some secondary corundum.

The main part of the iron content of the samples in the glassy phase is localized in the form of Fe^{2+} in network modifier positions, for all network former positions should be occupied by Al^{3+} ions as the better glass formers.

For reasons of comparison, glassy phases of the composition II in Fig. 1 were separately generated under addition of Fe_2O_3 and measured (Fig. 12). The result after the melting on exposure to air is an Fe^{3+} spectrum with $g' \approx 4.2$ typical of glasses, from which one can deduce rhombic symmetry of the Fe^{3+} positions. In addition one can observe fractions of magnetic order (broad resonances and a weak absorption at $g' \approx 2.1$) which imply the existence of Fe^{2+} ions. Annealing of these glassy phases (1000° C) produces a very wide EPR line which indicates the separation of an independent Fe–O phase ("Fe_2O_3"). This result corresponds to the formation of sample A_4 (see Fig. 10).

For a better imitation of the conditions during the melting and cooling down of the glassy phase-containing corundum materials, the separately produced glassy phase was additionally fused at 1200° C under reductive conditions and slowly cooled down. Under these conditions only partial Fe^{3+} reduction but also Na_2O vaporization (see Table I) are caused and aluminia (identified by X-ray phase analysis) separates from this now Al_2O_3-oversaturated melt and it contains Fe^{3+} ions in the lattice. This Fe^{3+} concentration is higher than those in any other samples discussed, and according to De Biast and Rodrigues [4, 5] it may be estimated at ≈ 0.5 wt %. The trend towards the incorporation of Fe^{3+} is higher under the aforementioned fusing conditions although there is a decline of the Fe^{3+} concentration in the glassy phase corresponding to the reduction (see Fig. 12). Generally, the Al^{3+} ions are slightly better glass-formers than Fe^{3+} and occupy network-former positions. On the other hand, α-Al_2O_3 is produced from the glass melt through crystallization and is able to incorporate Fe^{3+} during the slow cooling down. These conditions

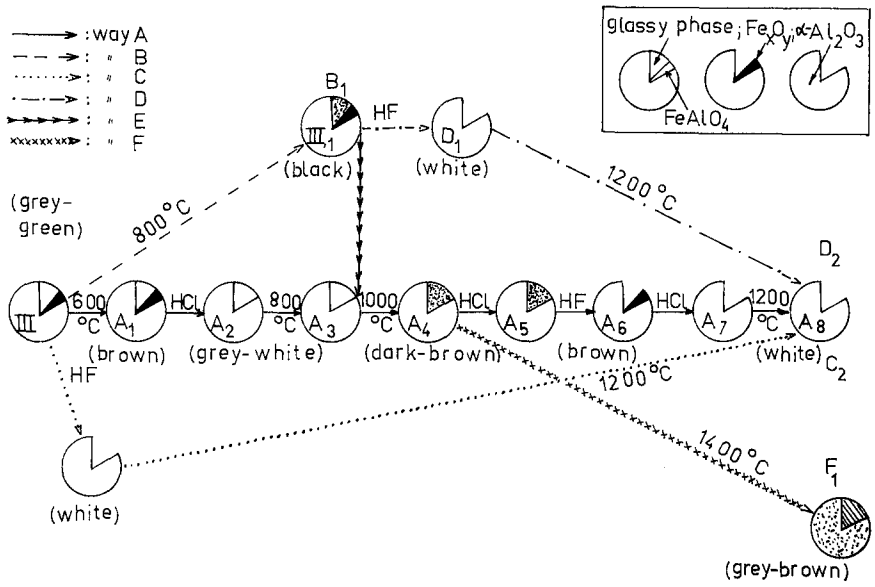

Figure 11 Treatments of sample III in different ways; the segments represent the phases (see inset) in a slightly overaccentuated manner.

are more favourable for the Fe^{3+} incorporation than a diffusion of Fe_2O_3 admixed into the corundum at 1350° C sample [4, 5].

3.5. Thermal, mechanical, and chemical treatment of sample III

This combined treatment was carried out under two aspects: Simulation of the thermal load on the materials, and identification of the existence, localization and transition of Fe^{2+} or other Fe–O_x phases. Sample III served as a model systems because it was expected to show the biggest changes. For clarity a scheme is given in Fig. 11. At first the compact sample III was pulversized in the W_2C beaker ("way A") and subsequently annealed at 600 or 700° C. The samples are stained markedly brown and yield an additional broad EPR signal ($g' \approx 2, \Delta B = 0.1$ to 0.2 T). In this temperature range the decomposition of a hercynite phase $FeAl_2O_4$ to Fe_2O_3 and Al_2O_3 or respective precursors is expected. A further thermal treatment of powders changes the Fe(II)/Fe(III) ratio as shown in Table I and indicates an overall oxidation of Fe(II). In contrast to this, the deep black sample III_1 is produced in way B through annealing of the compact material at 800° C. It shows typical magnetic order phenomena [20] and allows the conclusion of an existing magnetite phase (see also Figs 4 and 6).

Treatment of the brown sample A_1 with HCl results in a grey-white product with a scarcely modified α-Al_2O_3 or glassy phase, but Fe_2O_3 precursors were eliminated. Thus the colour essentially originates from these precursors. Furthermore, it is possible to conclude a relatively independent Fe(II)–O phase.

Further annealing at 800° C does not change the colour of the sample A_2. After renewed annealing at 1000° C the colour is deep brown which cannot extinguished by HCl. Sample A_4 is obtained in way B after the pulverization of III_1 or B_1 and subsequent annealing at 1000° C (way E) and shows typical signals of Fe^{3+} in the glass with $g' \approx 4.3$, Fe^{3+} in the α-Al_2O_3 as well as a broad resonance at $g \approx 2$ and 2.1 besides lines of impurities. The brown phase is not soluble in HF (A_5 by which the assumption of an Fe_2O_3-like phase is further corroborated. This Fe–O_x phase is separated from the glassy phase though HF treatment (A_6); however, it dissolves in HCl, and a white powder remains as sample A_7 (α-Al_2O_3/Fe^{3+}). So it is obvious that the glassy phase in sample III contained Fe^{2+}. Further heat treatment of A_7 does not change the colour of the sample but leads to a considerable increase ($\approx 5\times$) in the intensity of the signals of the Fe^{3+} in the α-Al_2O_3 (A_8). What must be considered essential reasons for this are the restitution process of the α-Al_2O_3 structure of the primary and secondary corundum as well as the oxidation of the Fe(II) (e.g. hercynite $FeAl_2O_4$) contained in solid solution [12, 15, 16].

What essentially results after grinding and HF treatment of III_1 – if way B is continued as way D – is a white corundum phase only, which – after annealing at 1200° C – shows the aforementioned effect in view of the Fe^{2+} and Fe^{3+} ions in the α-Al_2O_3.

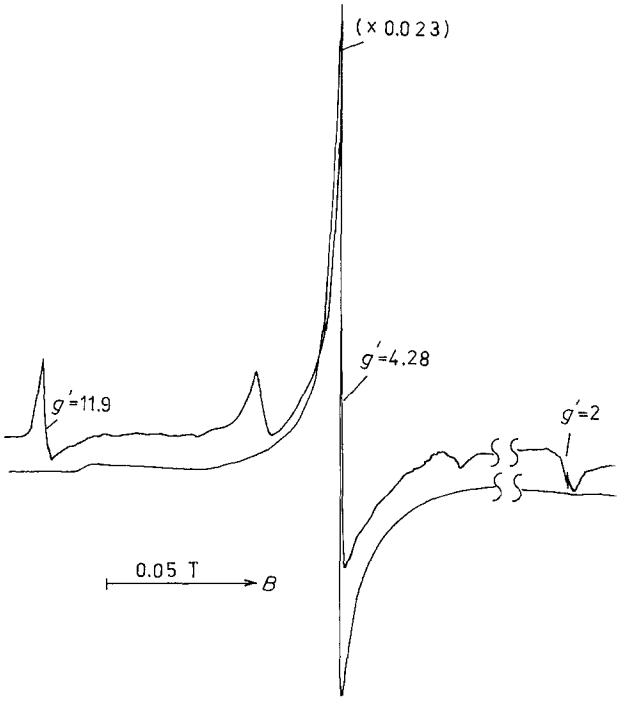

Figure 12 ESR spectra of the separately fused glassy phase; the upper curve shows the product after treatment (1200° C) under reductive conditions.

Since the oxidation in the compact III_1 does not yield Fe_2O_3, and independent "Fe_3O_4" phase or respective settings in the glassy phase are formed (see also Figs 4 and 5). The "magnetite" precursors contained in III_1 (or B_1) in contrast to Fe_2O_3 can be dissolved in HF and are extracted from the system together with the glassy phase.

Way C corroborates the statements made so far; after grinding of the compact material and its treatment with HF a white sample (α-Al_2O_3) (C_1) remains, that does not change its colour after the annealing at 1200° C and behaves like sample A_8 or D_2 (see above). If sample A_4 is annealed at 1400° C a grey-brown colour will result because of the existence of an Fe_2O_3 phase and its transition into "magnetite" which begins at this temperature (see also Fig. 3) and [18, 19]. The respective EPR spectrum is characterized by broad lines and a temperature dependence typical of magnetite precursors. At the same time the heat treatment at 1400° C increases the intensity of the signals of Fe^{3+} in the α-Al_2O_3 lattice whereby the lines grow broader by the factor of about 10. This effect is in accordance with published work [4, 5] as well as with our own studies regarding the diffusion of the Fe^{3+} ions from the admixed Fe_2O_3 into the corundum, which occurs at 1200° C to a low degree only but takes place successfully at 1350° C.

4. Conclusions

There is a reduction of the existing iron compounds in connection with the production of the initial melt in the composition according to Fig. 1 and with the parameters according to Fig. 2. Samples fused in a rigorously reductive way do not show any EPR signals of Fe^{3+} in the corundum or in the glassy phase, but there are Fe^0 domains with ferromagnetic properties. In loss reductive fusion conditions there is – at first, during the cooling down of the melt – a crystallization of the mixed crystals α-Al_2O_3/Fe_2O_3 and α-Al_2O_3/ $FeAl_2O_4$ whereby – in the course of the further cooling down–the solid solution corundum/ hercynite partly segregates according to the FeO–Al_2O_3 phase diagram (Fig. 1).

Simultaneously Fe^{2+} is partially oxidized in the residual melt because of its exposure to the air, and there is a slight increase in the available Fe^{3+}. A glassy phase containing some secondary corundum is separated. The concentration of the Fe^{3+} ions in the primary corundum depends on the speed of the cooling down of the melt or casting and on the amount of Fe^{3+} contained in the melt.

The line-widths of the EPR signals of the α-Al_2O_3/ Fe^{3+} are scarcely influenced by the cooling-down conditions. The variations detected in the Fe^{3+} concentrations (0.03 to 0.1 wt %) have no marked effect of ΔB_{pp}.

Heat treatment of the samples will result in the following changes of the iron species. They hercynitic phase existing in comparatively low concentrations is oxidized at around 600° C provided that enough oxygen is avialable. The reaction products yielded are Fe_2O_3 or its precursors, and Al_2O_3. Annealing of the compact material at temperatures around the transformation temperature of the glassy phase leads to settings of secondary corundum and magnetite in the glassy phase, whereby the latter remains black. This phenomenon does not occur with slowly cooled samples.

A large proportion of the Fe^{2+} ions is inserted into the glassy phase as network modifiers. The glassy phase is saturated with Al^{3+} and therefore does not take up much Fe^{3+}. At temperatures around 1000° C the oxidation of the Fe^{2+} ions results in the separation of independent Fe–O phases, preferably as Fe_2O_3. These phases are converted into magnetite-like phases at temperatures around 1400° C.

The intensities of the EPR signals of the Fe^{3+} in the corundum increase considerably at 1200° C. This indicates an oxidation of the hercynite contained in the corundum in solid solution because other iron pools do not exist.

The distinct diffusion of Fe^{3+} from the glassy phase or independent phases into the corundum begins at temperatures higher than 1350° C. The colour of the material is determined by the vitreous phase or the phases separated in it. Due to its low Fe^{3+} content the corundum is white in any case. Mechanical, thermal, and chemical aftertreatment of the samples in combination with the applied methods of investigation make it possible to obtain an indication of the localization of the oxidizable species (Fe^{2+} in the glass, $FeAl_2O_4$ and a solid solution of hercynite in the corundum) as well as on the coordination of the Fe^{3+} ions. The following model with regard to the localization of the iron species ensues:

Fe^{3+}: corundum, Fe_2O_3, Fe_3O_4 glassy phase;
Fe^{2+}: glassy phase, $FeAl_2O_4$, solid solution corundum/hercynite, Fe_3O_4;
Fe^0: (Fe^0) domains with ferromagnetic properties.

Oxidizable phases are of essential importance for the breaking strength of the materials under consideration.

References

1. A. S. HARE and J. C. VIKERMANN, *J. Chem. Soc., Faraday Trans. I* **77** (1981) 1103.
2. *Idem, ibid.* **77** (1981) 113.
3. R. S. De BIASI and D. C. S. RODRIGUES, *J. Mater. Sci.* **16** (1981) 968.
4. *Idem, J. Mater. Sci. Lett.* **2** (1983) 210.
5. *Idem, J. Amer. Ceram. Soc.* **68** (1985) 409.
6. E. F. OSBORNE and A. MUAN, in "Phase Equilibrium Diagrams of Oxide Systems" (Ceramic Foundation/Orton Jr, Columbus, Ohio, 1960).
7. W. A. FISCHER and A. HOFFMANN, *Arch . Eisenhütt.* **27** (1956) 343.
8. F. D. RICHARDSON and J. H. E. JEFFERS, "Thermodynamics of Solids", edited by R. A. Water, (Wiley, New York, 1961).
9. R. STÖSSER, R. BRENNEIS and I. EBERT, to be published.
10. R. STÖSSER, W. SCHWARZE and J. PREIDEL, *Z. Phys. Chem. (Leipzig)* **255** (1974) 895.
11. L. S. KORNIENKO and A. M. PROCHOROV, *J. Exp. Theoret. Phys.* **33** (1957) 805 (in Russian).
12. *Idem, ibid.* **40** (1961) 1594.
13. R. D. DOWSING and J. F. GIBSON, *J. Chem. Phys.* **50** (1969) 294.
14. R. AASA, *ibid.* **52** (1970) 3919.
15. YA. G. DORFMAN, *J. Exp. Theoret. Phys.* **48** (1965) 715

(in Russian).
16. C. A. BATES and P. STEGGLES, *J. Phys. C; Solid State Phys.* **8** (1975) 2283.
17. G. LEHMANN and H. HARDER, *Amer. Mineral.* **55** (1970) 98.
18. J. KVAPIL, *Krist. Techn.* **3** (1968) 665.
19. A. ROUSSET and J. PARIS, *Bull. Soc. Chim. Fr.* (1972) 3829.
20. YU. B. OSIPOV, "Magnetism Glinistych Gruntov" (Nedra, Moskva, 1978) (in Russian).

Received 21 August
and accepted 1 December 1987